

# From $\bar{K}N$ Interactions to $\bar{K}$ -Nuclear Quasi-Bound States

Aleš Cieplý,<sup>1, a)</sup> Jaroslava Hrtánková,<sup>1</sup> Jiří Mareš,<sup>1</sup>  
Eliahu Friedman,<sup>2</sup> Avraham Gal,<sup>2</sup> and Àngels Ramos<sup>3</sup>

<sup>1)</sup>*Nuclear Physics Institute of the Czech Academy of Sciences, 250 68 Řež, Czech Republic*

<sup>2)</sup>*Racah Institute of Physics, The Hebrew University, 91904 Jerusalem, Israel*

<sup>3)</sup>*Facultat de Física, Universitat de Barcelona, Martí i Franquès 1, 08028 Barcelona, Spain*

<sup>a)</sup>*Corresponding author: cieply@ujf.cas.cz*

**Abstract.** We review the current status of our study of  $K^-$ -nuclear interactions and  $K^-$ -nuclear quasi-bound states. The adopted  $K^-$ -nuclear optical potential consists of two parts – the single-nucleon one constructed microscopically from chirally motivated  $\bar{K}N$  amplitudes, and a phenomenological multi-nucleon one constrained in fits to kaonic atoms data. The inclusion of multi-nucleon absorption in our calculations of  $K^-$  quasi-bound states in many-body systems leads to huge widths, considerably exceeding the binding energies. If this feature is confirmed the observation of such states is unlikely. Finally, a development of a new microscopical model for in-medium  $K^-NN$  absorption is discussed as well.

## INTRODUCTION

The interactions of (anti)kaons with nucleons and nuclei represent an interesting topic related (among others) to SU(3) chiral symmetry, structure of composite systems or even to content of strangeness in hot and dense nuclear matter as studied in astrophysics. Here we review the recent progress in calculations of the characteristics of  $K^-$ -nuclear quasi-bound states using the  $K^-$ -nuclear optical potential constrained in fits to kaonic atoms data. The single-nucleon part of the potential is constructed as a coherent sum of  $K^-N$  scattering amplitudes,  $V_{K^-}^{1N} \sim t_{K^-N}(\rho)\rho$ , where  $\rho$  denotes the nuclear density and in-medium t-matrices are derived from the free-space ones by accounting for Pauli blocking. Strong energy dependence of the scattering amplitudes is treated self-consistently, iterating the energy at which the  $K^-N$  (and  $K^-$ -nuclear) amplitude is evaluated. We note that in-medium hadron self-energies are disregarded in the present report as their inclusion would require a more complex treatment going beyond using the free space  $K^-N$  amplitudes as input in our calculations. The self-consistent procedure leads to substantial downward energy shift, typically about 30 MeV or even as large as 50-100 MeV in calculations of  $K^-$ -atomic or  $K^-$ -nuclear states, respectively. The details of the procedure can be found e.g. in [1, 2, 3].

It was demonstrated in [2] that the optical potential  $V_{K^-}^{1N}$  does not provide a satisfactory description of the kaonic atoms data and has to be supplemented with a part related to kaon interactions with two or more nucleons. In close similarity with earlier pion-nuclear studies, a phenomenological term  $V_{K^-}^{mN}$  was considered in [2],

$$2\text{Re}(\omega_{K^-})V_{K^-}^{mN} = -4\pi B(\rho/\rho_0)^\alpha \rho, \quad (1)$$

where  $\omega_{K^-} = m_{K^-} - B_{K^-} - i\Gamma_{K^-}/2$  stands for (a complex) kaon energy,  $B_{K^-}$  ( $\Gamma_{K^-}$ ) denotes the  $K^-$  binding energy (width),  $m_{K^-}$  is the  $K^-$  mass and  $\rho_0 = 0.17 \text{ fm}^{-3}$ . The complex parameter  $B$  determines the strength of the  $V_{K^-}^{mN}$  potential that simulates processes on two nucleons or in general any *multi-nucleon* contributions to the total optical potential,  $V_{K^-} = V_{K^-}^{1N} + V_{K^-}^{mN}$ .

When calculating the  $K^-$ -atomic or  $K^-$ -nuclear states, the interaction of the  $K^-$  meson with a nucleus is described by the Klein-Gordon equation

$$\left[ \vec{\nabla}^2 + \tilde{\omega}_{K^-}^2 - m_{K^-}^2 - \Pi_{K^-}(\omega_{K^-}, \rho) \right] \phi_{K^-} = 0, \quad (2)$$

where  $\tilde{\omega}_{K^-} = \omega_{K^-} - V_C$  with  $V_C$  standing for the Coulomb potential. The kaon self-energy is related directly to the  $K^-$ -nuclear optical potential,  $\Pi_{K^-}(\omega_{K^-}, \rho) = 2\text{Re}(\omega_{K^-})V_{K^-}$ . Finally, we note that as the optical potential is constructed from the  $\bar{K}N$  amplitudes evaluated at energies affected (in nuclear matter) by the kaon self-energy, the potential itself as well as the in-medium energy shift it causes are to be calculated self-consistently.

## CHIRALLY MOTIVATED $\bar{K}N$ AMPLITUDES

A modern treatment of low-energy meson-baryon interactions is provided by approaches based on chiral perturbation theory combined with coupled channel T-matrix re-summations techniques. The parameters of such models are fitted to low energy  $K^-p$  total cross sections, the threshold branching ratios (see e.g. [?] ) and to the strong-interaction characteristics of the  $1s$  level in kaonic hydrogen measured recently by the SIDDHARTA collaboration [4]. Several theoretical groups presented models describing about equally well this set of experimental data. We refer to these approaches as Kyoto-Munich (KM) [5], Prague (P) [6], Bonn (B2, B4) [7], Murcia ( $M_I$ ,  $M_{II}$ ) [8] and Barcelona (BCN) [9], with some of them providing two solutions. The first four models are compared in [10].

In Fig. 1 we present the predictions of the models for  $K^-p$  and  $K^-n$  elastic amplitudes in the free space. Concerning the  $K^-p$  amplitude, all these *state-of-the-art* chiral models are in agreement in a region of energies at and above the  $K^-p$  threshold. The only exception is the Bonn approach due to different treatment of off-shell effects and partial waves. The above models yield considerably different  $K^-p$  amplitude below the threshold. On the other hand, for the  $K^-n$  amplitude the model variations are quite large over the whole energy region. The reason is that the  $I = 1$  amplitudes, as well as the subthreshold  $K^-p$  amplitudes, are not sufficiently restricted by the experimental data.

In nuclear matter the free-space  $K^-N$  amplitudes are modified due to Pauli blocking and hadron self-energies, the latter effectively modifying the in-medium hadron masses as well. It appears that for energies at least about 20 MeV below the  $\bar{K}N$  threshold the main effect comes from the Pauli blocking and can be approximated by a simple multiplication of the free-space  $K^-N$  amplitudes by an energy and density dependent factor derived from considering

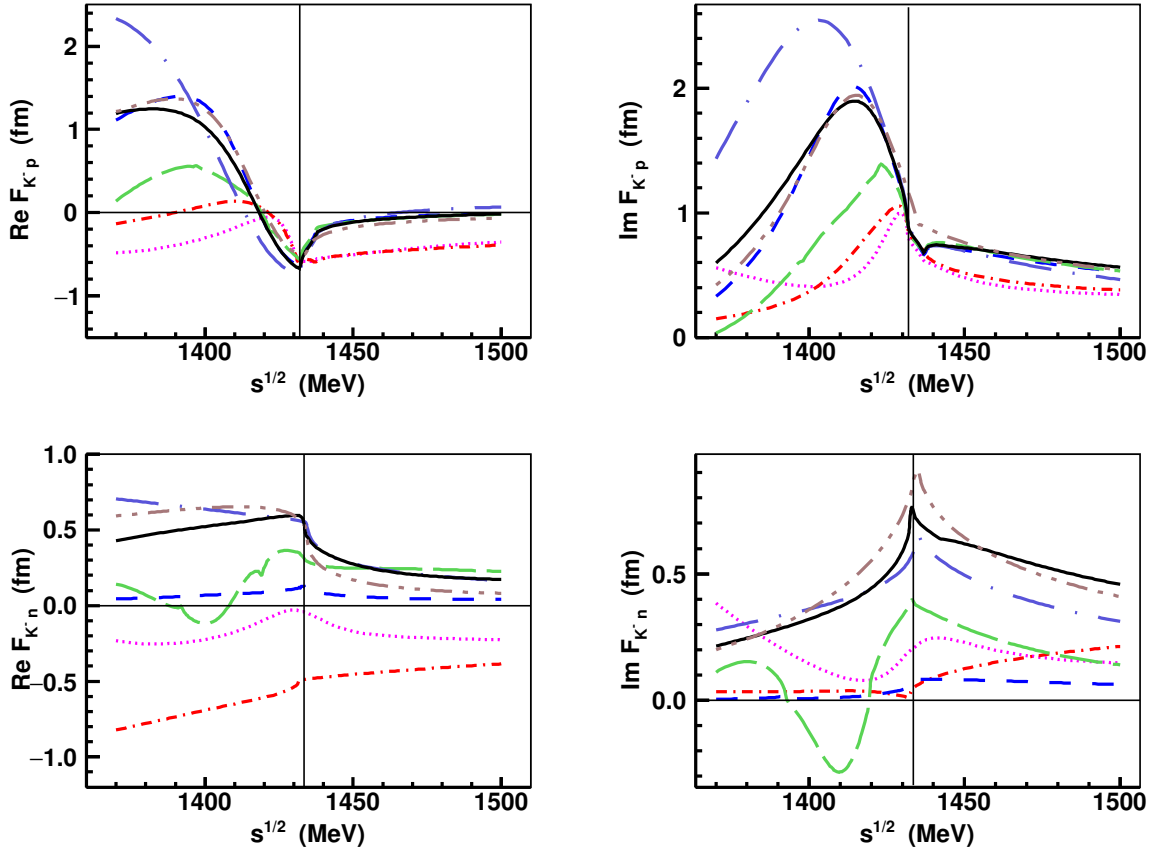


**FIGURE 1.** The  $K^-p$  (top panels) and  $K^-n$  (bottom panels) elastic scattering amplitudes generated by recent chirally motivated approaches. The various lines refer to the models: B2 (dotted, purple), B4 (dot-dashed, red),  $M_I$  (dashed, blue),  $M_{II}$  (long-dashed, green), P (dot-long-dashed, violet), BCN (dot-dot-dashed, brown), and KM (continuous, black). The thin vertical lines in the panels mark the pertinent  $K^-N$  thresholds.

nucleon-nucleon anti-correlations [2, 3, 11].

## KAONIC ATOMS

The data base for kaonic atoms comprises of 65 experimental results for strong interaction level shifts and widths of so-called *lower states* and relative yields of transitions from so-called *upper states* to the lower states [12]. This data set was used in fits performed in [2] with several versions of the  $K^-$ -nuclear optical potential. First, it was found that the potential  $V_{K^-}^{IN}$  constructed self-consistently from the in-medium  $\bar{K}N$  amplitudes fails miserably when used to calculate the  $K^-$ -atomic characteristics. However, good fits to the data were obtained for all models augmented with the phenomenological  $V_{K^-}^{mN}$  term. We refer the reader to [2] and [13] for more details on the analysis and fitting procedure. Here we only mention that due to correlations between  $\alpha$  and the complex  $B$  parameter, that define the form and strength of the  $mN$  term, it was necessary to scan over the parameter  $\alpha$  when searching for the best  $\chi^2$  value while varying the  $B$  parameter.

In Table I we show the results of the fits performed with the Prague, Kyoto-Munich and Barcelona models. For these fits, the  $\alpha$  parameter was fixed at values very close to the best fit ones with the variations in  $B$  reflecting the model uncertainties. The achieved total  $\chi^2$  values are very similar for all models including the Bonn and Murcia ones. The latter ones are omitted in Table I as they do not satisfy an additional constraint of reproducing single-nucleon absorption fractions (SNAF) measured in bubble-chamber experiments on several nuclei from C to Br long time ago [14, 15, 16]. A common experimental value  $\text{SNAF}_{\text{exp}} = 0.75 \pm 0.05$  was adopted in [2] as a further test for the input  $\bar{K}N$  models. While the B and M models were found to significantly underestimate the SNAF value, the other three models based on the P, KM and BCN amplitudes comply nicely with it as demonstrated in Fig. 2. There, the P and KM model predictions almost coincide, so we opted to show lines that represent both models in the left panel of Fig. 2.

**TABLE I.** The parameters and total  $\chi^2$  values obtained in fits to kaonic atoms data. For the optical potentials based on the P and KM amplitudes two versions of density dependence were considered in the phenomenological  $mN$  term, tagged as P $\alpha$  and KM $\alpha$ , respectively.

	P1	KM1	BCN	P2	KM2
$\alpha$	1	1	1	2	2
Re $B$ (fm)	$-1.3 \pm 0.2$	$-0.9 \pm 0.2$	$-1.3 \pm 0.3$	$-0.5 \pm 0.6$	$0.3 \pm 0.7$
Im $B$ (fm)	$1.5 \pm 0.2$	$1.4 \pm 0.2$	$1.9 \pm 0.3$	$4.6 \pm 0.7$	$3.8 \pm 0.7$
$\chi^2(65)$	125	123	129	125	123

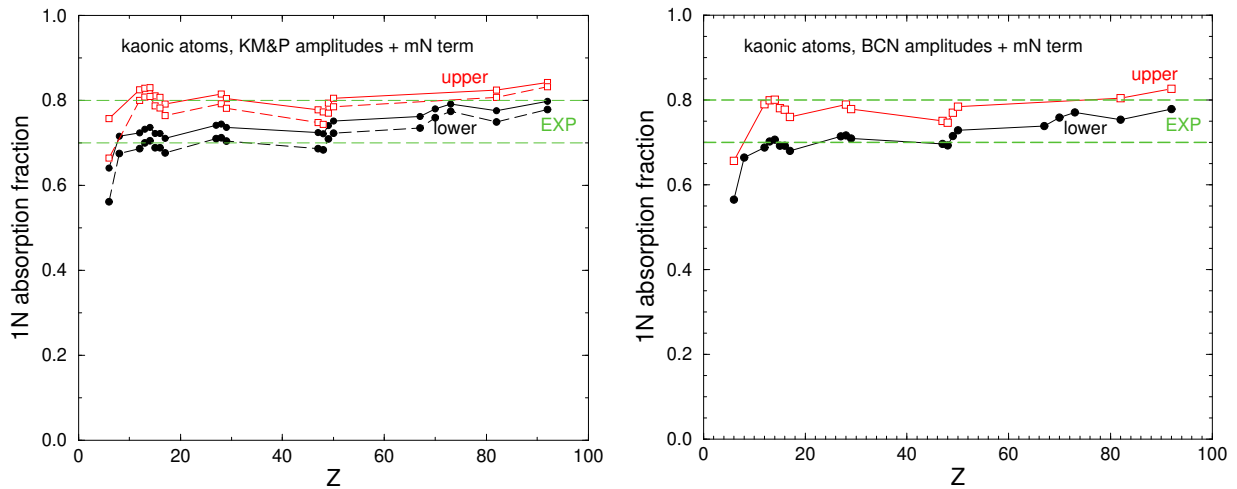


**FIGURE 2.** Left panel: Calculated SNAF for the P and KM models,  $\alpha = 1$  (solid line) and  $\alpha = 2$  (dashed line) [2]. Right panel: SNAF for the BCN model. The solid circles and open squares stand for *lower* and *upper*  $K^-$ -atomic states, respectively.

## KAONIC NUCLEI

The formalism outlined above was adopted to self-consistent calculations of  $K^-$ -nuclear quasi-bound states in selected nuclei across the periodic table [3, 17]. The nucleus was described within a relativistic mean field model. It was demonstrated in the analysis of kaonic atoms [2] that the optical potential  $V_{K^-}$  is not so well determined at densities larger than about 30-50% of the nuclear density  $\rho_0$ . For this reason, two scenarios were adopted in calculations of the  $K^-$ -nuclear states. In the *full density* (FD) option the  $V_{K^-}^{mN} \sim B(\rho/\rho_0)^\alpha \rho$  form was used in the entire nucleus, while in the *half density* (HD) option the  $mN$  term was fixed at a constant value equal to  $V_{K^-}^{mN}(0.5\rho_0)$  for densities  $\rho \geq 0.5\rho_0$ . In addition, the amplitude  $\text{Im}B$  in Eq. (1) was multiplied by a kinematical suppression factor to account for phase space reduction. More details can be found in [3, 17].

In Fig. 3 we compare the contributions of the  $1N$  (denoted KN) and  $mN$  (denoted KNN) parts in the KM1 version of the optical potential. Both parts are calculated self consistently for the  $^{208}\text{Pb}$  nucleus. The  $1N$  component of the optical potential notably differs from the input  $1N$  term (green solid lines) owing to different subthreshold energy shifts obtained upon including (or excluding) the  $mN$  phenomenological term. The marked uncertainties reflect the variations in the  $mN$  input strength parameter  $B$  determined in kaonic atoms fit and noted in Table I. Whereas the resulting real potential depths are considerably lower than those obtained in totally phenomenological analyses [18], the imaginary potentials are dominated by the  $mN$  component and become extremely deep, close to 160 MeV (and much more in the KM2 optical potential). The dominance of the  $mN$  component over the  $1N$  one is also realized in most of the other models based on the chirally motivated  $\bar{K}N$  amplitudes employed in [3].

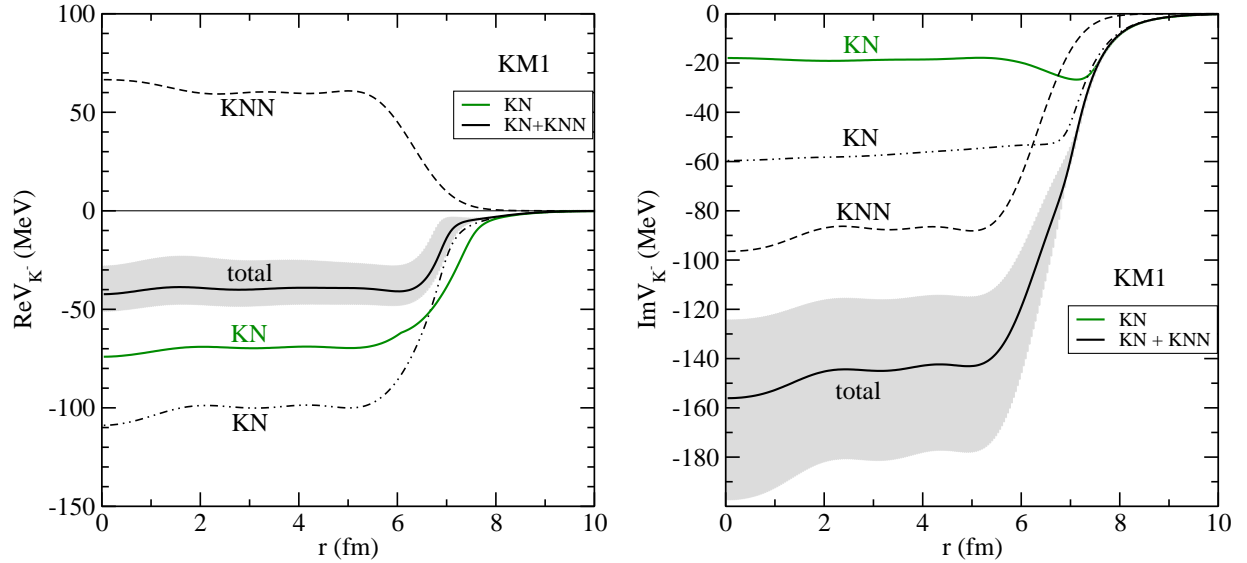


**FIGURE 3.** The contributions from  $V_{K^-}^{1N}$  and  $V_{K^-}^{mN}$  potentials to the total real and imaginary  $K^-$  optical potential in the  $^{208}\text{Pb}+K^-$  nucleus, calculated self-consistently in the KM1 model and for the FD variant. The single-nucleon  $K^-$  potential (green solid line) of the KM model is shown for comparison. Shaded area represent uncertainties in the phenomenological  $mN$  part input.

In Fig. 4 we present individual contributions of the  $K^-$  single-nucleon (dashed lines) and multi-nucleon (solid lines) absorption to the total  $K^-$  absorption, expressed as a fraction of  $\text{Im}V_{K^-}^{1N}$  and  $\text{Im}V_{K^-}^{mN}$  with respect to the total imaginary potential  $\text{Im}V_{K^-}$  in  $^{208}\text{Pb}$ , calculated self-consistently within the KM1 model for the HD (red) and FD (black) options. The nuclear density distribution  $\rho/\rho_0$  (thin dotted line) is shown for comparison. Both versions of the  $V_{K^-}^{mN}$  potential give very similar fractions of single- and multi-nucleon absorption at low densities as well as in the nuclear interior. Since the range and density dependence of the corresponding potentials are different, the relative contribution of  $\text{Im}V_{K^-}^{1N}$  and  $\text{Im}V_{K^-}^{mN}$  to the  $K^-$  absorption is changing with radius (density), as expected. While at the nuclear surface, the dominant process is the  $K^-$  absorption on a single nucleon, in the nuclear interior the  $1N$  absorption is reduced due to the vicinity of the  $\pi\Sigma$  threshold and the  $mN$  absorption prevails.

In Table II the binding energies  $B_{K^-}$  and absorption widths  $\Gamma_{K^-}$  are presented for the  $1s$  levels in several  $K^-$ -nuclei across the periodic table, as calculated within the P and KM models. In the KN columns we also show the binding energies and widths obtained when only the  $1N$  term is used in the optical potential. The inclusion of the  $mN$  term

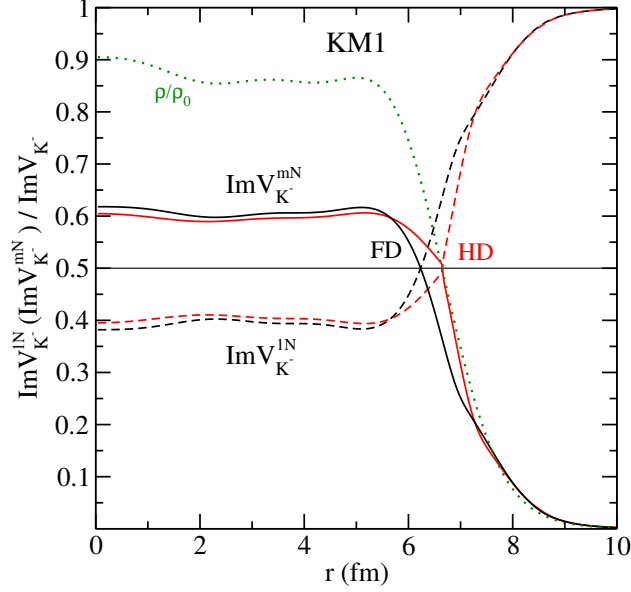


**FIGURE 4.** Ratios of  $\text{Im}V_{K^-}^{1N}$  and  $\text{Im}V_{K^-}^{mN}$  potentials to the total  $\text{Im}V_{K^-}$  as a function of radius, calculated self-consistently for  $^{208}\text{Pb}+K^-$  system in the KM1 model and different options for the  $K^-$  multi-nucleon potential.

leads to a drastic increase of  $K^-$  widths while  $K^-$  binding energies are affected only moderately. For most kaonic nuclei the HD option of the  $V_{K^-}^{mN}$  potential yields  $K^-$  widths of about 100 MeV while the binding energies are much smaller than the pertinent widths. The situation is much worse for the FD version of the optical potential that even does not predict any  $K^-$  bound state in the majority of nuclei. Therefore, our results suggest that the widths of  $K^-$ -nuclear quasi-bound states are considerably larger than their binding energies, at least for nuclei with  $A \geq 10$ . This makes an experimental observation of such states very unlikely.

**TABLE II.**  $1s$   $K^-$  binding energies  $B_{K^-}$  and widths  $\Gamma_{K^-}$  (in MeV) in various nuclei calculated within the KM and P models with the  $V_{K^-}^{1N}$  potential (denoted KN); plus a phenomenological  $V_{K^-}^{mN}$  term for the HD $\alpha$  and FD $\alpha$  options (see text for details).

		KM model					P model				
		KN	HD1	FD1	HD2	FD2	KN	HD1	FD1	HD2	FD2
$^{16}\text{O}$	$B_{K^-}$	45	34	not	48	not	64	49	not	63	not
	$\Gamma_{K^-}$	40	109	bound	121	bound	25	94	bound	117	bound
$^{40}\text{Ca}$	$B_{K^-}$	59	50	not	64	not	81	67	not	82	not
	$\Gamma_{K^-}$	37	113	bound	126	bound	14	95	bound	120	bound
$^{208}\text{Pb}$	$B_{K^-}$	78	64	33	80	53	99	82	36	96	47
	$\Gamma_{K^-}$	38	108	273	122	429	14	92	302	117	412

## $\bar{K}NN$ IN-MEDIUM ABSORPTION

The introduction of the phenomenological  $V_{K^-}^{mN}$  potential was essential for a successful description of  $K^-$ -atomic data. However, one may argue that an energy-dependent two-nucleon potential of a different form could do the job as well, and may not lead to such a drastic increase of the predicted decay widths of the  $K^-$ -nuclear states. In this Section we briefly report on a development of a microscopical model describing the  $K^-$  absorption on two nucleons in nuclear matter. The formalism follows closely the approach adopted in [19] to derive the  $\eta'NN$  optical potential. The  $K^-$  absorption on two nucleons is described within a meson-exchange picture with the  $K^-NN$  self-energy modeled using

chirally motivated  $\bar{K}N$  amplitudes modified due to Pauli blocking. In actual calculations, the P and BCN models were used providing a comparison of the results and a measure of the sensitivity to a particular  $\bar{K}N$  model.

We do not dwell on technical details of the  $\bar{K}NN$  model here as they are prepared for publication elsewhere [20]. Instead, we promote the work by picking one result to demonstrate the applicability of the model. It relates to a recent AMADEUS measurement of the  $\Lambda p$  to  $\Sigma^0 p$  production rate in  $K^- NN$  quasi-free absorption reported in [21],

$$R = \frac{\text{BR}(K^- pp \rightarrow \Lambda p)}{\text{BR}(K^- pp \rightarrow \Sigma^0 p)} = 0.7 \pm 0.2(\text{stat.})_{-0.3}^{+0.2}(\text{sys.}). \quad (3)$$

In Fig. 5 taken from [20] we show the ratio predicted with the new  $\bar{K}NN$  model when either the free space (black lines) or Pauli blocked (red lines)  $\bar{K}N$  amplitudes are employed. The density dependence of the rate is presented using the P and BCN amplitudes for two settings of the  $\bar{K}NN$  model, assuming the  $K^-$  binding energy in nuclear matter to be either  $B_{K^-} = 0$  or  $B_{K^-} = 50 \rho/\rho_0$  MeV. In the experimentally relevant region of densities, the ratio  $R$  calculated with Pauli blocked amplitudes turns out smaller and in better agreement with the measured value. This feature manifests the relevance of medium modifications of the chirally motivated amplitudes.

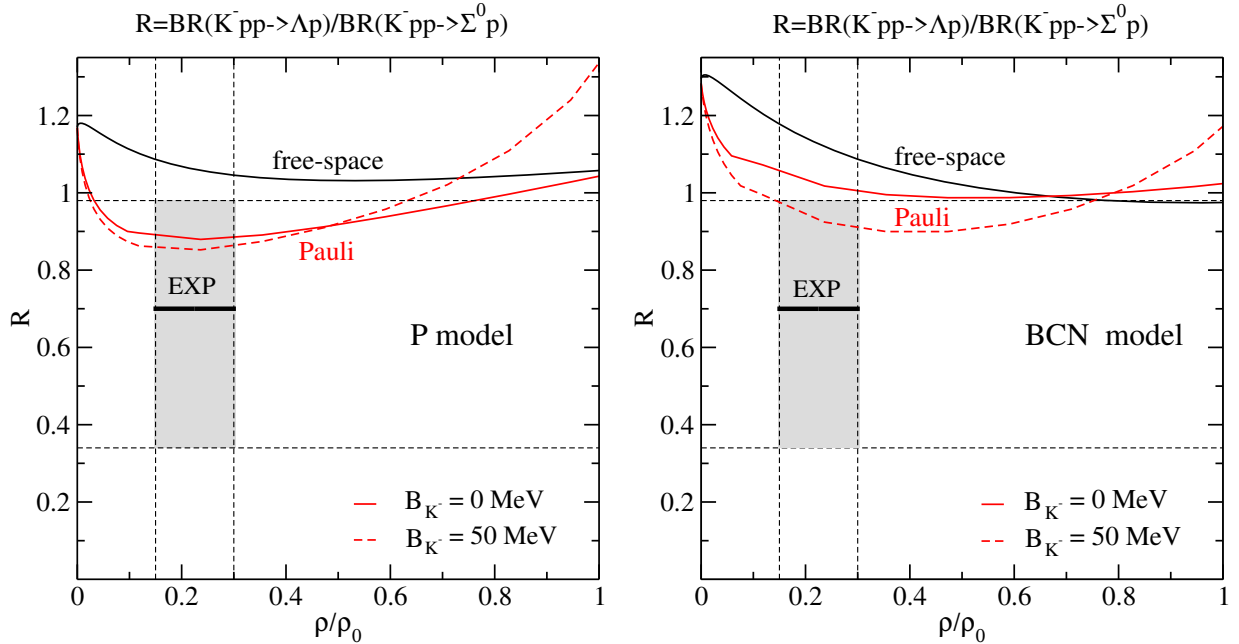


**FIGURE 5.** The ratio of branching ratios for the in-medium  $K^- pp \rightarrow \Lambda p$  and  $K^- pp \rightarrow \Sigma^0 p$  reactions. The gray rectangle marks an estimated region of densities probed by low-energy antikaons and the experimental error band. Left - P model, right - BCN model.

## BRIEF SUMMARY

- The up-to-date (NLO) chirally motivated  $\bar{K}N$  models provide very different predictions for the  $K^- N$  amplitudes at subthreshold energies. As in-medium kaons probe energies as far as 50-100 MeV below the  $\bar{K}N$  threshold a realistic treatment of the energy dependence including Pauli blocking is essential.
- $K^-$  optical potentials derived from chirally-inspired  $K^- N$  interaction models need to be supplemented by an additional phenomenological density-dependent term representing  $K^-$  multi-nucleon interactions in order to get satisfactory global fit to kaonic-atom strong-interaction data. The P, KM and BCN models are favored satisfying the additional constraint of  $1N$  to  $mN$  absorption rate.

- The inclusion of multi-nucleon absorption in the calculations of  $K^-$  quasi-bound states in many-body systems leads to huge widths, considerably exceeding the binding energies. If this feature is confirmed the observation of such states is unlikely. The conclusion does not necessarily apply to few body  $K^-$ -nucleons systems.
- A microscopical model for  $K^-NN$  absorption in nuclear matter has been developed using chirally motivated  $\bar{K}N$  amplitudes. The results look encouraging, the ratio of  $\Lambda p$  to  $\Sigma^0 p$  production measured by AMADEUS is reproduced by the model when the in-medium amplitudes are employed.

## ACKNOWLEDGMENTS

This work was supported by the Czech Science Foundation GACR grant 19-19640S.

## REFERENCES

1. A. Cieplý, E. Friedman, A. Gal, D. Gazda, and J. Mareš, Phys. Rev. **C84**, 045206 (2011).
2. E. Friedman and A. Gal, Nucl. Phys. **A959**, 66–82 (2017).
3. J. Hrtánková and J. Mareš, Phys. Rev. **C96**, 015205 (2017).
4. M. Bazzi et al., Phys. Lett. **B704**, 113–117 (2011).
5. Y. Ikeda, T. Hyodo, and W. Weise, Nucl. Phys. **A881**, 98–114 (2012).
6. A. Cieplý and J. Smejkal, Nucl. Phys. **A881**, 115–126 (2012).
7. M. Mai and U.-G. Meißner, Eur. Phys. J. **A51**, 30 (2015).
8. Z.-H. Guo and J. A. Oller, Phys. Rev. **C87**, 035202 (2013).
9. A. Feijoo, V. Magas, and A. Ramos, Phys. Rev. **C99**, 035211 (2019).
10. A. Cieplý, M. Mai, U.-G. Meißner, and J. Smejkal, Nucl. Phys. **A954**, 17–40 (2016).
11. T. Waas, M. Rho, and W. Weise, Nucl. Phys. **A617**, 449–463 (1997).
12. E. Friedman and A. Gal, Phys. Rept. **452**, 89–153 (2007).
13. E. Friedman, EPJ Web Conf. **199**, 01013 (2019).
14. H. Davis, F. Oppenheimer, W. L. Knight, F. R. Stannard, and O. Treutler, Nuovo Cimento **LIII**, 313 (1968).
15. J. W. Moulder, N. E. Garrett, L. M. Tucker, W. M. Bugg, G. T. Condo, H. O. Cohn, and R. D. Mcculloch, Nucl. Phys. **B35**, 332–350 (1971).
16. C. Vander Velde-Wilquet, J. Sacton, J. H. Wickens, D. N. Tovee, and D. H. Davis, Nuovo Cimento **A39**, 538 (1977).
17. J. Hrtánková and J. Mareš, Phys. Lett. **B770**, 342–247 (2017).
18. J. Mareš, E. Friedman, and A. Gal, Nucl. Phys. **A770**, 84–105 (2006).
19. H. Nagahiro, S. Hirenzaki, E. Oset, and A. Ramos, Phys. Lett. **B709**, 87–92 (2012).
20. J. Hrtánková and A. Ramos, submitted to Phys. Rev. C (2019), arXiv:1910.01336 [nucl-th].
21. R. Del Grande et al., Eur. Phys. J. **C79**, 190 (2019).